Title

Ester modification at the 3′ end of anti-microRNA oligonucleotides increases potency of microRNA inhibition

Authors

Pham, Kevin M
Suter, Scott R
Lu, Shannon S
et al.

Publication Date

2021

DOI

10.1016/j.bmc.2020.115894

Peer reviewed

HHS Public Access

Author manuscript

Bioorg Med Chem. Author manuscript; available in PMC 2021 November 23.

Published in final edited form as:

Bioorg Med Chem. 2021 January 01; 29: 115894. doi:10.1016/j.bmc.2020.115894.

Ester Modification at the 3' End of Anti-MicroRNA Oligonucleotides Increases Potency of MicroRNA Inhibition

Kevin M. Pham, **Scott R. Suter**, **Shannon S. Lu**, **Peter A. Beal***

Department of Chemistry, University of California, One Shields Avenue, Davis, CA 95616, United States

Abstract

MicroRNAs (miRNAs) are short noncoding RNAs that play a fundamental role in gene regulation. Deregulation of miRNA expression has a strong correlation with disease and antisense oligonucleotides that bind and inhibit miRNAs associated with disease have therapeutic potential. Current research on the chemical modification of anti-miRNA oligonucleotides (anti-miRs) is focused on alterations of the phosphodiester-ribose backbone to improve nuclease resistance and binding affinity to miRNA strands. Here we describe a structure-guided approach for modification of the 3'-end of anti-miRs by screening for modifications compatible with a nucleotide-binding pocket present on human Argonaute2 (hAgo2). We computationally screened a library of 190 triazole-modified nucleoside analogs for complementarity to the t1A-binding pocket of hAgo2. Seventeen top scoring triazoles were then incorporated into the 3' end of anti-miR21 and potency was evaluated for each in a cell-based assay for anti-miR activity. Four triazole-modified anti-miRs showed higher potency than anti-miR21 bearing a 3' adenosine. In particular, a triazole-modified nucleoside bearing an ester substituent imparted a nine-fold and five-fold increase in activity for both anti-miR21 and anti-miR122 at 300 and 5 nM, respectively. The ester group was shown to be critical as a similar carboxylic acid and amide were inactive. Furthermore, anti-miR 3' end modification with triazole-modified nucleoside analogs improved resistance to snake venom phosphodiesterase, a 3'-exonuclease. Thus, the modifications described here are good candidates for improvement of anti-miR activity.

Keywords

RNA interference; microRNA; anti-microRNA; click chemistry; molecular docking; Argonaute2

1. Introduction

MicroRNAs (miRNAs) are small, ~22 nucleotide endogenous noncoding RNAs that play a fundamental role in post-transcriptional gene regulation.[1] Briefly, a miRNA strand is loaded into an Argonaute (Ago) protein and the resulting ribonucleoprotein (RNP) complex binds mRNAs with complementarity to the miRNA seed region (nucleotides 2–8).[2] This results in repression of translation, deadenylation and degradation of the target mRNA.[3] MiRNAs regulate genes involved in a wide variety of cellular processes.[4] However, deregulation of

*Corresponding Author: pabeal@ucdavis.edu.

certain miRNAs is correlated with human diseases such as cancer, inflammation, central nervous system disorders, metabolic diseases, and more.[5] These observations have spurred efforts to develop miRNA-based therapeutics.

One approach to the development of miRNA therapeutics is the use of antisense oligonucleotides (anti-miRs) to target miRNAs whose elevated levels are associated with disease.[5] Research in anti-miR design has been primarily focused on chemically modifying the sugar or phosphodiester backbone of the oligonucleotide to improve nuclease resistance and thermodynamic stability of the miRNA/anti-miR duplex.[6] For example, phosphorothioate (PS) linkages and 2'-O-methyl modifications of anti-miRs have been shown to improve nuclease resistance.[7,8] Locked nucleic acid (LNA) modifications that pre-organize the sugar into a 3'-endo pucker allow binding to miRNA with extremely high affinity.[9–13] There are other recent reports of anti-miR design strategies implemented to improve potency and nuclease resistance.[14–17]

Since the active fraction of a miRNA in a cell is associated with an Ago protein, structures of Ago proteins bound to RNA provide a potential starting point for further anti-miR optimization. The crystal structure of human Ago2 (hAgo2) with bound miRNA and target RNA (Fig. 1a) expanded our understanding of the molecular mechanisms underlying miRNA target recognition.[18,19] Several key features of miRNA recognition within hAgo2 were discovered, including the binding of the 5' end of the miRNA strand into the MID domain and 3' end into the PAZ domain that allows cradling of the miRNA-target duplex.[18] One intriguing structural feature of hAgo2 is a small solvated pocket within the L2 and MID domains of hAgo2 that has specific binding to adenosine present on the target strand at nucleotide position 1 (t1A) (Fig. 1b). Since miRNAs bind anti-miRs in a manner similar to target strand recognition, the t1 nucleotide position corresponds to the 3' end of a typical anti-miR. The specificity for adenosine in the t1A pocket is likely due to hydrogen bonding interactions with the N6 amine of adenine by Ser561 and a network of ordered water molecules within the pocket (Fig. 1b). Furthermore, modifications of adenosine in the target RNA strand were used to confirm this specificity through *in vitro* binding, crystallography, and FRET assays.[20]

We previously used structure-based modifications of small interfering RNAs (siRNAs) to improve potency and reduce miRNA-like off targeting effects.[21–23] For instance, modifying the 5' position of an siRNA guide strand using click chemistry with prior computational screening of triazole ligands docked into the MID domain improved potency and gene silencing efficacy.[24] Here, we use this strategy to improve the potency of anti-miRs. Using the structure of hAgo2 with bound miRNA-target RNA duplex, we computationally screened a library of triazole-modified nucleotides and selected high scoring candidates for further study. We performed copper-catalyzed alkyne/azide cycloaddition (CuAAC) reactions to generate high scoring t1-triazole-modified anti-miRs and determined their potency in cell-based anti-miR assays. We identified several triazole-modified anti-miRs that are more potent than anti-miRs bearing an adenosine at the t1 site. One modification caused a significant increase in potency. Subsequent structure-activity relationship studies revealed the importance of an ester-bearing side chain on the triazole. This ester modification was

found to increase potency for two different anti-miR sequences. Furthermore, we found that triazole-modified anti-miRs showed increased 3'-exonuclease resistance.

2. Results and Discussion

2.1 Design and synthesis of anti-miR21 bearing t1-triazole modifications

To test anti-miR modifications, we chose to target miR-21, an abundant miRNA in HeLa cells.[25] We evaluated potency of modified anti-miRs using a previously reported dual luciferase assay wherein Renilla luciferase protein expression is under the control of miR-21 since the miR-21 target sequence has been inserted into the 3'-UTR of the Renilla transcript.[26] Functional anti-miRs that inhibit miR-21 activity increase Renilla luciferase signal in this assay. We evaluated the potency of a variety of anti-miR-21 designs, including: sequence lengths of 9 nucleotides complementary to the miR-21 seed region, 15 nucleotides, and a 22mer fully complementary to the miR-21 guide strand; backbone modifications of 2'-O-methyl or locked nucleic acid (LNA) to improve nuclease resistance and binding affinity towards miR-21; and, substituting adenine at the t1 position with other bases such as guanine, cytosine, uracil, and 2,6-diaminopurine. Ultimately, we chose a 15 mer, fully 2'-O-methylated anti-miR-21 with a 1'-ethynyl-2'-deoxyribose nucleotide at position t1 that could serve as a precursor for triazoles via CuAAC reactions (Fig. 2). Based on previous reports[27,28], a 15 mer anti-miR21 was sufficient for binding to miR21-loaded Ago2 without promoting release of the miR21 from Ago2.[29] A C3 spacer controlled pore glass (CPG) reagent and 1'-ethynyl-2'-deoxyribose phosphoramidite were used to incorporate the alkyne at the anti-miR-21 t1 position. We found that neither the 2'-deoxyribose sugar nor the 1-ethynyl-2'-deoxyribose modification negatively impacted potency (Fig. S1), indicating that the 15 mer anti-miR21 precursor was appropriate for click modifications after computationally screening t1 nucleotide triazoles.

2.2 Computational screening of triazole-modified nucleotides

We used the *OpenEye* program suite to computationally screen a library of 1'-triazole nucleotide ligands bearing a variety of different substituents for complementarity with the t1A-binding pocket of hAgo2. In short, we designed a library of triazole ligands with substituents that could be rapidly incorporated at the t1 position of anti-miR21 using readily available azides, generated conformers of each molecule in the library, then docked the conformers into a rigid receptor that defines the t1A-binding pocket from the published crystal structure of hAgo2 with bound guide and target RNA duplex (PDB file 4W5O). A detailed description of the docking procedure can be found in the Methods section. After docking a library of 190 triazoles (Fig. S2 and Table S1), we narrowed down our potency screening to 17 triazole candidates (Fig. 3). In addition, 2'-deoxyadenosine (dA), 2'-deoxycytidine (dC), 2'-deoxyguanosine (dG), 2'-deoxyuridine (dU), 2'-deoxy-2,6-diaminopurine (dDAP), and 1'-ethynyl-2'-deoxyribose (dER) bisphosphate ligands were docked into the pocket to serve as control ligands.[20]

The 17 candidates were chosen based on docking score (ChemGauss4) and orientation in the binding pocket as well as availability of the azides from commercial sources. The ChemGauss4 scoring function uses smooth Gaussian potentials to map ligand atoms into a

receptor site and recognize interactions such as hydrogen bonding from ligand to protein, hydrogen bonding of ligand to implicit solvent, shape interactions, and metal chelation, all as a function of a distance, to generate scores.[37] A more negative Chemgauss4 score indicates a more favorable docked ligand into the receptor site. In general, larger ligands did not dock well into the small t1A-binding pocket receptor and pointed out towards the solvent or away from the pocket, resulting in poor scores. Ligands that docked well were heterocyclic, aromatic, or contained at least one hydrogen bonding group. The scores of each of the top 17 triazole candidates were from 10- to 20-fold higher than the docked 2'-deoxyadenosine. The candidates all provided adequate space filling in the t1A pocket receptor and most have the potential to engage in hydrogen-bonding interactions with the protein side chains. These significantly higher docked scores gave reason for us to pursue triazole modifications on anti-miR21 that would contain each of the 17 substituents.

2.3 Anti-miR21 bearing triazoles at the t1 position show improved potency in HeLa cells

With the 17 lead compounds identified, we proceeded with CuAAC reactions on t1 1'-ethynyl anti-miR21 to generate each triazole. We then obtained a potency profile of all the triazole-modified anti-miR21s from 25 to 300 nM concentration in HeLa cells along with co-transfected miR-21 reporter plasmid (Fig. 4). We found that four triazole-modified anti-miR21s show a higher level of activity relative to anti-miR21 containing a t1 adenine (Fig. 4). Interestingly, the methyl acetate triazole anti-miR21 exhibited a nearly 4-fold higher activity level at 25 nM to upwards of nearly 9-fold higher activity level relative to no anti-miR control at 300 nM. The methyl furan, thiophene and furan triazoles also showed increased potency compared to adenine (Fig. 4). Interestingly, the activities of the triazole-modified anti-miR21 oligonucleotides do not directly correlate with the docking scores for the top 17 ligands from the computational screening (Fig. 3). Thus, this approach appears to be best suited for rapid, qualitative screening for candidate modifications with follow up testing planned for several high scoring hits. The highly potent methyl acetate modification generated numerous poses with the ester side chain directed at the t1A-binding pocket of hAgo2 (see Fig. S3 for top pose). Due to the substantial increase in activity seen with the methyl acetate modification, we carried out additional structure-activity relationship studies to identify the key features.

2.4 Structure activity relationships for ester triazole-modified anti-miR21

We attempted to define the important features of the ester-modified anti-miR21 using two approaches. One approach was to replace the methyl ester with other similar functional groups. The other approach was to test whether the ester modification affects potency when placed on the 5'-end of the anti-miR21 instead of the 3'-end.

When the methyl acetate substituent is replaced with an ethyl acetate, the potency slightly improves (Fig. 5). The basis for this small enhancement is not known at this time. Interestingly, an N-ethylacetamide-modified triazole did not show the large increase in activity seen with the esters (Fig. 5).

We explored the possibility that the ester substituent on anti-miR21 could undergo hydrolysis during endocytosis into HeLa cells[30], resulting in a free acid. However, a 3'

acetic acid modification also resulted in no potency enhancement indicating that an intact ester is required for the effect. We also determined potency of the anti-miR21 with the ester modification present on the 5’ end instead of the 3’ end. Interestingly, anti-miR21 with either the methyl ester or ethyl ester modification showed a small increase in activity above the control, with a 2 to 4-fold higher activity observed. Further experiments would need to be done to explore the possibility of an additive improvement of potency when both the 5’ and 3’ end are modified with an ester. Nonetheless, the impact of the ester modifications on the 5’-end is significantly lower than 3’-end modified anti-miR21 (Fig. 5). In addition, the 5’ N-ethylacetamide triazole-modified anti-miR21 showed no increase in potency, consistent with its activity when present at the 3’-end.

2.5 T1-triazole modifications on anti-miR122 improves potency in HuH-7 cells

Since we had identified a highly active triazole modification for the t1 position of anti-miR21, we wished to determine if this modification could enhance activity of other anti-miRs. Therefore, we measured the potency of t1 triazole-modified anti-miR122 capable of de-repressing miR-122 targets in liver carcinoma HuH-7 cells.[31–33]

We first designed a 15 mer anti-miR122 that was fully 2’-O-methylated and contained the 1’-ethynyl-2’-deoxyribose at t1 nucleotide. Our initial potency results in HuH-7 cells showed near-background levels of activity with adenine as the t1 nucleobase (Fig. S4). To increase the overall potency of the anti-miR122 in the assay, we replaced the 2’-O-methyl uridine nucleotides with locked nucleic acid thymidine (LNA T) (Fig. 6a). Replacing 2’-O-methyl nucleotides with LNA nucleotides is known to increase anti-miR potency.[34] With this design, further modification with either the ethyl ester or methyl furan triazole resulted in improvement in activity relative to t1 1’-ethyne control (Fig. 6b). Thus, the pattern of the activity found for the triazole modifications with anti-miR21 was also observed with anti-miR122. Furthermore, the N-ethylacetamide t1 triazole-modified anti-miR122 showed baseline levels of activity comparable to 1’-ethyne control, again indicating that the ester modifications are more active over the others tested.

Overall, the data indicate that the triazole modifications enhance activity in a different anti-miR sequence, as well as with backbone chemical modifications (2’-O-Me and LNA) that are currently being used in oligonucleotide therapeutics. It is notable that the fold difference in potency for the methyl furan triazole modification of anti-miR122 is higher while the ethyl ester substituent on the triazole of anti-miR122 is lower than the potencies of modified anti-miR21 (Fig. 4 and 5). This could be due to differences in abundance of endogenous miR-122 in HuH-7 cells compared to miR-21 in HeLa cells. We performed a follow up control experiment to determine if anti-miR21 was specific for miR21 in HeLa cells in comparison to anti-miR122 (Fig. S5). The results showed that there was no activity from ethyl ester-modified anti-miR122 targeting miR21 in HeLa cells. In addition, we found that modified anti-miR21 had no activity for targeting miR122 in HuH-7 cells (Fig. S4).

2.6 Modifications at the anti-miR t1 position reduce reactivity to a 3’-exonuclease

We performed a snake venom phosphodiesterase (SVPD) assay (see Supplementary Methods for assay conditions) using triazole-modified anti-miR21s as substrates to test

the effect of t1 modifications on 3'-exonuclease reactivity. After 48 hours of incubation in 0.01 U/mL SVPD, the anti-miR21 with t1 adenine showed complete degradation to shorter products (Fig. S6). However, when the anti-miR21 contained a 1'-triazole or 1'-ethynyl group on the t1 nucleotide, intact oligonucleotide is nearly fully retained. This significant increase in 3'-exonuclease resistance may be due to the C-nucleoside nature of the t1 nucleotide that is not easily recognized by 3'-exonuclease.[35] However, it is important to note that even triazole-modified anti-miRs that showed no improvement in anti-miR activity, namely the triazoles with chlorobenzene and N-ethylacetamide substituents, still exhibited high levels of SVPD resistance. This suggests the increased anti-miR potency is not solely due to improved resistance to 3'-exonuclease.

2.7 Binding analysis of miR-21-loaded hAgo2 with chemically modified anti-miR21 using a biotin pulldown assay

We wished to determine whether our anti-miR modifications improved potency by directly increasing binding affinity to miRNA-loaded hAgo2. For this purpose, we used a pulldown assay with 5'-biotinylated anti-miR21 (Fig. S7a) bearing different 3' end modifications and human cell lysates containing miR21-loaded hAgo2 (see Supplementary Methods for assay conditions). However, while the assay results clearly indicated that the modified anti-mR21 oligonucleotides bound miR21-loaded hAgo2 (i.e. a scrambled sequence control showed less hAgo2 pulled down), no differences were observed between the anti-miRs with different 3' end modifications (Fig. S7b). Thus, at this time, we have not unequivocally established that the novel 3' end modifications reported here increase hAgo2 binding affinity. It is possible that the hAgo2 affinity differences for the differently modified anti-miRs are too small to be observed with this assay system or the differences in anti-miR activity observed here arise from effects other than changes in binding affinity to hAgo2. The improved activity could come from a variety of other sources including improved binding to other human Argonaute proteins with structurally similar t1-binding pockets (e.g. hAgo1)[36] or from effects on the efficiency of anti-miR transfection. Additional studies will be required to fully elucidate the origin(s) of the improved anti-miR activity reported here.

2.8 Conclusions

In conclusion, we have described novel chemical modifications for anti-miRs that improve potency of miRNA inhibition in cultured human cells. Computational screening of a library of triazole-modified nucleoside analogs docked into the hAgo2 t1A-binding pocket identified candidates that were subsequently shown to impart improvement in potency for both anti-miR21 and anti-miR122. The anti-miRs modified at the 3' end with a nucleoside analog bearing an ester substituent substantially improved potency over other substituents tested. Several nucleoside analogs described here improved resistance to a model 3' exonuclease (SVPD), but this effect is unlikely to fully explain the origin of the improvement in activity. Overall, this study expands the repertoire of anti-miR chemical modification strategies to improve potency of miRNA inhibition.

3. Materials and Methods

3.1 Dual luciferase reporter plasmid generation

The miR-21 and miR-122 reporter plasmids were generated by inserting the miR-21 (5'-TCAACATCAGTCTGATAAGCTA-3') and miR-122 (5'-ACAAACACCATTGTCACACTCCA –3') target sequences into the 3'-untranslated region (3'-UTR) of the renilla luciferase gene (*hRluc*) in dual luciferase reporter plasmid psiCHECK-2 (Promega), respectively. Primers containing either the miR-21 or miR-122 target sequences (Table S2) were amplified with psiCHECK-2 template using the Phusion Hot Start II DNA Polymerase kit (Thermo Scientific) to generate PCR product with overlapping regions for Gibson assembly. The miR-21 or miR-122 reporter plasmid PCR product was combined with Gibson Assembly Master Mix (New England Biolabs) and incubated at 50 °C for 15 minutes then transformed into XL10-Gold® Ultracompetent Cells (Agilent Technologies) according to the manufacturer's instructions. XL10-Gold cells harboring miR-21 or miR-122 reporter plasmid were inoculated in 100 μg/mL ampicillin-containing LB media for antibiotic resistance selection. Finally, miR-21 or miR-122 reporter plasmids were harvested from XL10-Gold cells using the PureYield™ Plasmid Miniprep System (Promega) and Sanger sequenced by the UC DNA Sequencing Facility at UC Davis for sequence verification.

3.2 Cell culture

HeLa (ATCC CCL-2) and HuH-7 (Japanese Collection of Research Bioresources, JCRB0403), and HEK293T (ATCC, CRL-3216) cells were cultured in Dulbecco's modified Eagle medium (DMEM, Gibco 11995065) supplemented with 10% fetal bovine serum (FBS, Gibco) and 100X antibiotic-antimycotic solution (Anti-Anti, Gibco 15240062) to a final concentration of 10% and 1X, respectively, at 37 °C + 5% CO_2. All cells were passaged regularly to maintain exponential growth.

3.3 Cell transfection and dual luciferase assay

HeLa or HuH-7 cells were plated onto a 96-well plate at 1×10^4 cells per well in DMEM supplemented with 10% FBS and 1X Anti-Anti solution 24 h before transfection. The following day, the cells were co-transfected in triplicate with varying concentrations of anti-miR oligonucleotide and 100 ng of dual luciferase reporter plasmid, miR-21 reporter or miR-122 reporter, using Lipofectamine 2000 (Invitrogen) according to the manufacturer's instructions in 100 μL reduced serum media (OPTI-MEM, Gibco) per well. After 6 h incubation post-transfection, the reduced serum media was replaced with DMEM supplemented with 10% FBS. After an additional 18 h post-transfection, 24 h total, the cells were lysed and luciferase luminescent counts were measured using the Dual Luciferase Assay System (Promega). Briefly, the transfected cells were washed with phosphate buffer saline (PBS, Gibco) followed by addition of 20 μL 1X Passive Lysis Buffer (Promega) and gentle shaking on an orbital shaker for 15 minutes. Next, 100 μL of luciferase assay reagent II (LARII, Promega) was added to each well of lysed cells to measure firefly luciferase luminescent counts on a CLARIOstar Plus microplate reader (BMG Labtech). Stop & Glo Reagent (100 μL) (S&G, Promega) was subsequently added to quench firefly luciferase activity and measure renilla luciferase luminescent counts. For each luminescent

count reading, there is a 2 s pre-measurement delay, followed by a 10 s measurement period. Finally, the renilla luciferase luminescent counts were normalized against firefly luciferase luminescent counts and plotted as a fold change in the ratio of Renilla/Firefly (RL/FF) counts relative to cells transfected with reporter plasmid, but without anti-miR oligonucleotide as a control.

3.4 Oligonucleotide preparation

All anti-miR oligonucleotides were ordered through Dharmacon (Lafayette, CO), TriLink BioTechnologies (San Diego, CA), or synthesized in the laboratory. Anti-miR122 oligonucleotides with locked nucleic acid (LNA) T and 1'-ethynyl-2'-deoxyribose modifications at the 3' end and 5'-biotinylated anti-miR21 and anti-miR122 oligonucleotides were synthesized using the Applied Biosystems (ABI) 394 DNA/RNA Synthesizer. The phosphoramidite and controlled pore glass (CPG) reagents used for synthesis were purchased from Glen Research. Oligonucleotides synthesized in the laboratory were cleaved from the 3'-Spacer C3 CPG columns using 2:1 of 30% NH_4OH and EtOH overnight. The cleaved oligonucleotide solution was transferred away from the CPG beads and concentrated to dryness using a SpeedVac concentrator then resuspended in nuclease free water and desalted using an illustra™ Nap™-10 Sephadex™ G-25 columns (GE Healthcare). All oligonucleotides were electrophoresed in a 19% polyacrylamide gel and extracted from the gel after UV shadowing. The oligonucleotide was then purified from the gel using the crush and soak method at 4 °C overnight in buffer containing 0.5 M NH_4OAc and 0.1 mM EDTA.[24] Finally, the oligonucleotides were ethanol precipitated or purified using SepPak C18 columns (Waters) with 1:1 CH_3CN/H_2O elution and characterized by MALDI-TOF mass spectrometric analysis. All oligonucleotide sequences and masses are reported in Supplementary Tables S3–S6.

3.5 Generation of t1-triazole modified anti-miR via copper(I)-catalyzed azide/alkyne cycloaddition (CuAAC) reaction

The procedure to generate triazole-modified anti-miRs is described previously.[24] In a 1.5 mL microcentrifuge tube, 0.88 μL of 100 mM $CuSO_4$ (88 nmol) dissolved in nuclease free water, was combined with 1.75 μL of 100 mM Tris(3-hydroxypropyltriazolylmethyl)amine (THPTA, 175 nmol), also dissolved in nuclease free water, and incubated for 5 min at room temperature. (+)-Sodium L-ascorbate (1.75 μL of 100 mM, 175 nmol), in nuclease free water, was then added to the solution for reduction of Cu^{2+} to Cu^{+}, where a blue-to-clear solution color change is observed. Next, 1.05 μL of 100 mM azide (105 nmol), dissolved in DMSO, was added to the solution and mixed well by pipetting. DMSO (6 μL) of was added to the solution to facilitate miscibility and reduce precipitation of azide in the reaction tube. HEPES pH 7 buffer (6.07 μL of 100 mM) was used to dissolve 3.5 nmol of dried-down alkyne-modified anti-miR oligonucleotide and transferred to the reaction tube, resulting in a total reaction volume of 17.5 μL. The solution was incubated for ~2.5 h at room temperature then quenched using 17.5 μL of 80% formamide loading buffer (80% formamide, 10 mM EDTA, 0.05% xylene cyanol FF, and 0.05% bromophenol blue in MilliQ®-purified water). To purify the CuAAC oligonucleotide product, the quenched reaction was loaded into a denaturing (8 M urea) 19% PAGE gel and electrophoresed for ~3 h at 20W. After electrophoresis, the oligonucleotide bands were crushed and soaked as

described above. The oligonucleotide was either ethanol precipitated or purified using a SepPak C18 cartridge. Lastly, the purified oligonucleotide products were characterized by MALDI-TOF spectrometric analysis. Note that CuAAC reactions were scaled 1.5- or 3-fold higher than what is reported here to generate more oligonucleotide product per reaction, as needed.

3.6 Computational screening of t1-triazole modified nucleotides docked into the t1A-binding pocket of hAgo2

T1-triazole modified nucleotides were docked into the t1A-binding pocket of hAgo2 using OpenEye Suite Scientific Software (New Mexico, USA).[24,37] The general procedure for docking is as follows:

1) Library generation: A library of 190 3’,5’-bisphophate ribose ligands with a triazole moiety at the 1’ position were drawn using ChemDraw then converted into SMILES format. The SMILES were uploaded onto VIDA to generate molecular models of the ligands. The triazoles designed were from a variety of azides that would be commercially available through Sigma Aldrich or Enamine LLC to conveniently obtain and test in the laboratory once triazole anti-miRs were generated.

2) Conformer generation: Conformers of the triazole ligands were generated using OMEGA. A maximum of 5,000 conformers per ligand were applied to allow a wide selection of conformers for each ligand to be docked into the receptor.

3) Receptor generation: The t1A-binding pocket of hAgo2 receptor was generated using the MakeReceptor program from OpenEye. Using the published crystal structure of hAgo2 with bound guide and target RNA (4W5O), an approximate 5,000 $Å^3$ box was encased around the t1A-binding pocket to create heavy atom contours. Constraints were applied to the reference t1-adenosine ligand (Fig. S8) to force the triazole 3’,5’-bisphosphate ligand to be positioned in the pocket.

4) Fast rigid exhaustive docking (FRED): Once the conformers of the triazole ligands and t1A-binding pocket receptor were made, all confomers of the triazoles were docked into the binding pocket using Fast Rigid Exhaustive Docking (FRED), available in OpenEye. The conformers were computationally scored by ChemGauss4 when docked into the receptor based on shape complementarity from ligand to receptor, hydrogen bonding between ligand and protein, and hydrogen bonding interactions with implicit solvent. A more negative score indicates a more favorable docking score. Each ligand had 25 poses assigned in the docking run.

5) Analysis of FRED poses and scoring: We sorted the docked poses from lowest (more favorable) to highest (least favorable) ChemGauss4 score and chose 17 triazoles from the top ~50 scoring ligands to determine their activity via the dual luciferase assay, based on availability of the azides and how consistent the 25 poses from each ligand were oriented towards the t1A-binding pocket receptor and overlapped with the t1-adenosine reference ligand.

Supplementary Material

Refer to Web version on PubMed Central for supplementary material.

Acknowledgements:

P.A.B. acknowledges the National Institutes of Health for financial support in the form of grant R01 GM080784. We would like to acknowledge Erin Doherty, Cody Palumbo, and Hannah Brinkman for generating MALDI-TOF mass spectra of all the anti-miR oligonucleotides. We would also like to acknowledge the UC Davis DNA Sequencing Facility for sequencing the reporter plasmids.

References:

(1). Gebert LFR; MacRae IJ Regulation of MicroRNA Function in Animals. Nat. Rev. Mol. Cell Biol 2019, 20 (1), 21–37. 10.1038/s41580-018-0045-7. [PubMed: 30108335]

(2). Fabian MR; Sonenberg N The Mechanics of MiRNA-Mediated Gene Silencing: A Look under the Hood of MiRISC. Nat. Struct. Mol. Biol 2012, 19 (6), 586–593. 10.1038/nsmb.2296. [PubMed: 22664986]

(3). Wilson RC; Doudna JA Molecular Mechanisms of RNA Interference. Annu. Rev. Biophys 2013, 42 (1), 217–239. 10.1146/annurev-biophys-083012-130404. [PubMed: 23654304]

(4). Cai Y; Yu X; Hu S; Yu J A Brief Review on the Mechanisms of MiRNA Regulation. Genomics, Proteomics Bioinforma 2009, 7 (4), 147–154. 10.1016/S1672-0229(08)60044-3.

(5). Rooij E; Kauppinen S Development of Micro RNA Therapeutics Is Coming of Age. EMBO Mol. Med 2014, 6 (7), 851–864. 10.15252/emmm.201100899. [PubMed: 24935956]

(6). Lennox KA; Behlke MA Chemical Modification and Design of Anti-MiRNA Oligonucleotides. Gene Ther 2011, 18 (12), 1111–1120. 10.1038/gt.2011.100. [PubMed: 21753793]

(7). Eckstein F Phosphorothioates, Essential Components of Therapeutic Oligonucleotides. Nucleic Acid Ther 2014, 24 (6), 374–387. 10.1089/nat.2014.0506. [PubMed: 25353652]

(8). Sproat BS; Lamond AI; Beijer B; Neuner P; Ryder U Highly Efficient Chemical Synthesis of 2′-O-Methyloligoribonucleotides and Tetrabiotinylated Derivatives; Novel Probes That Are Resistant to Degradation by RNA or DNA Specific Nucleases. Nucleic Acids Res 1989, 17 (9), 3373–3386. 10.1093/nar/17.9.3373. [PubMed: 2726482]

(9). Singh SK; Nielsen P; Koshkin AA; Wengel J LNA (Locked Nucleic Acids): Synthesis and High-Affinity Nucleic Acid Recognition. Chem. Commun 1998, 455–456.

(10). Wengel J; Koshkin A; Singh SK; Nielsen P; Meldgaard M; Rajwanshi VK; Kumar R; Skouv J; Nielsen CB; Jacobsen JP; et al. LNA (Locked Nucleic Acid): Synthesis of the Adenine, Cytosine, Guanine, 5-Methylcytosine, Thymine and Uracil Bicyclonucleoside Monomers, Oligomerisation, and Unprecedented Nucleic Acid Recognition. Nucleosides and Nucleotides 1999, 18 (6–7), 1365–1370. 10.1080/07328319908044718.

(11). Obika S; Nanbu D; Hari Y; Morio KI; In Y; Ishida T; Imanishi T Synthesis of 2'-O,4'-C-Methyleneuridine and -Cytidine. Novel Bicyclic Nucleosides Having a Fixed C3'-Endo Sugar Puckering. Tetrahedron Lett 1997, 38 (50), 8735–8738. 10.1016/S0040-4039(97)10322-7.

(12). Petersen M; Nielsen CB; Nielsen KE; Jensen GA; Bondensgaard K; Singh SK; Rajwanshi VK; Koshkin AA; Dahl BM; Wengel J; et al. The Conformations of Locked Nucleic Acids (LNA). J. Mol. Recognit 2000, 13 (1), 44–53. 10.1002/(SICI)1099-1352(200001/02)13:1<44::AID-JMR486>3.0.CO;2-6. [PubMed: 10679896]

(13). Kaur H; Wengel J; Maiti S Thermodynamics of DNA-RNA Heteroduplex Formation: Effects of Locked Nucleic Acid Nucleotides Incorporated into the DNA Strand. Biochemistry 2008, 47 (4), 1218–1227. 10.1021/bi700996z. [PubMed: 18171024]

(14). Lennox KA; Owczarzy R; Thomas DM; Walder JA; Behlke MA Improved Performance of Anti-MiRNA Oligonucleotides Using a Novel Non-Nucleotide Modifier. Mol. Ther. - Nucleic Acids 2013, 2 (AUG), e117. 10.1038/mtna.2013.46. [PubMed: 23982190]

(15). Mie Y; Hirano Y; Kowata K; Nakamura A; Yasunaga M; Nakajima Y; Komatsu Y Function Control of Anti-MicroRNA Oligonucleotides Using Interstrand Cross-Linked Duplexes. Mol.

Ther. - Nucleic Acids 2018, 10 (March), 64–74. 10.1016/j.omtn.2017.11.003. [PubMed: 29499957]

(16). Yoshioka K; Kunieda T; Asami Y; Guo H; Miyata H; Yoshida-Tanaka K; Sujino Y; Piao W; Kuwahara H; Nishina K; et al. Highly Efficient Silencing of MicroRNA by Heteroduplex Oligonucleotides. Nucleic Acids Res 2019, 47 (14), 7321–7332. 10.1093/nar/gkz492. [PubMed: 31214713]

(17). Ariyoshi J; Momokawa D; Eimori N; Kobori A; Murakami A; Yamayoshi A Development of Novel Antisense Oligonucleotides for the Functional Regulation of RNA-Induced Silencing Complex (RISC) by Promoting the Release of MicroRNA from RISC. Bioconjug. Chem 2015, 26 (12), 2454–2460. 10.1021/acs.bioconjchem.5b00501. [PubMed: 26471458]

(18). Schirle NT; MacRae IJ The Crystal Structure of Human Argonaute2. Science 2012, 336 (6084), 1037–1040. 10.1126/science.1221551. [PubMed: 22539551]

(19). Schirle NT; Sheu-Gruttadauria J; MacRae IJ Structural Basis for MicroRNA Targeting. Science 2014, 346 (6209), 608–613. 10.1126/science.1258040. [PubMed: 25359968]

(20). Schirle NT; Sheu-Gruttadauria J; Chandradoss SD; Joo C; MacRae IJ Water-Mediated Recognition of T1-Adenosine Anchors Argonaute2 to MicroRNA Targets. Elife 2015, 4 (September), 1–16. 10.7554/eLife.07646.

(21). Jackson AL; Bartz SR; Schelter J; Kobayashi SV; Burchard J; Mao M; Li B; Cavet G; Linsley PS Expression Profiling Reveals Off-Target Gene Regulation by RNAi. Nat. Biotechnol 2003, 21 (6), 635–637. 10.1038/nbt831. [PubMed: 12754523]

(22). Jackson AL; Burchard J; Schelter J; Chau BN; Cleary M; Lim L; Linsley PS Widespread SiRNA "off-Target" Transcript Silencing Mediated by Seed Region Sequence Complementarity. Rna 2006, 12 (7), 1179–1187. 10.1261/rna.25706. [PubMed: 16682560]

(23). Burchard J; Jackson AL; Malkov V; Needham RHV; Tan Y; Bartz SR; Dai H; Sachs AB; Linsley PS MicroRNA-like off-Target Transcript Regulation by SiRNAs Is Species Specific. Rna 2009, 15 (2), 308–315. 10.1261/rna.1326809. [PubMed: 19144911]

(24). Onizuka K; Harrison JG; Ball-Jones AA; Ibarra-Soza JM; Zheng Y; Ly D; Lam W; Mac S; Tantillo DJ; Beal PA Short Interfering RNA Guide Strand Modifiers from Computational Screening. J. Am. Chem. Soc 2013, 135 (45), 17069–17077. 10.1021/ja4079754. [PubMed: 24152142]

(25). Lui WO; Pourmand N; Patterson BK; Fire A Patterns of Known and Novel Small RNAs in Human Cervical Cancer. Cancer Res 2007, 67 (13), 6031–6043. 10.1158/0008-5472.CAN-06-0561. [PubMed: 17616659]

(26). Obad S; Dos Santos CO; Petri A; Heidenblad M; Broom O; Ruse C; Fu C; Lindow M; Stenvang J; Straarup EM; et al. Silencing of MicroRNA Families by Seed-Targeting Tiny LNAs. Nat. Genet 2011, 43 (4), 371–380. 10.1038/ng.786. [PubMed: 21423181]

(27). Hogan DJ; Vincent TM; Fish S; Marcusson EG; Bhat B; Nelson Chau B; Zisoulis DG Anti-MiRs Competitively Inhibit MicroRNAs in Argonaute Complexes. PLoS One 2014, 9 (7). 10.1371/journal.pone.0100951.

(28). Ariyoshi J; Matsuyama Y; Kobori A; Murakami A; Sugiyama H; Yamayoshi A Effective Anti-MiRNA Oligonucleotides Show High Releasing Rate of MicroRNA from RNA-Induced Silencing Complex. Nucleic Acid Ther 2017, 27 (5), 303–308. 10.1089/nat.2017.0663. [PubMed: 28876213]

(29). De N; Young L; Lau PW; Meisner NC; Morrissey DV; MacRae IJ Highly Complementary Target RNAs Promote Release of Guide RNAs from Human Argonaute2. Mol. Cell 2013, 50 (3), 344–355. 10.1016/j.molcel.2013.04.001. [PubMed: 23664376]

(30). Geisow MJ; Evans WH PH in the Endosome. Measurements during Pinocytosis and Receptor-Mediated Endocytosis. Exp. Cell Res 1984, 150 (1), 36–46. 10.1016/0014-4827(84)90699-2. [PubMed: 6198190]

(31). Fukuhara T; Kambara H; Shiokawa M; Ono C; Katoh H; Morita E; Okuzaki D; Maehara Y; Koike K; Matsuura Y Expression of MicroRNA MiR-122 Facilitates an Efficient Replication in Nonhepatic Cells upon Infection with Hepatitis C Virus. J. Virol 2012, 86 (15), 7918–7933. 10.1128/jvi.00567-12. [PubMed: 22593164]

(32). Chang J; Nicolas E; Marks D; Sander C; Lerro A; Buendia MA; Xu C; Mason WS; Moloshok T; Bort R; et al. MiR-122, a Mammalian Liver-Specific MicroRNA, Is Processed from Hcr MRNA and May Downregulate the High Affinity Cationic Amino Acid Transporter CAT-1. RNA Biol 2004, 1 (2), 106–113. 10.4161/rna.1.2.1066. [PubMed: 17179747]

(33). Takahashi M; Yamada N; Hatakeyama H; Murata M; Sato Y; Minakawa N; Harashima H; Matsuda A In Vitro Optimization of 2′-OMe-4′-Thioribonucleoside-Modified Anti-MicroRNA Oligonucleotides and Its Targeting Delivery to Mouse Liver Using a Liposomal Nanoparticle. Nucleic Acids Res 2013, 41 (22), 10659–10667. 10.1093/nar/gkt823. [PubMed: 24030710]

(34). Fabani MM; Gait MJ MiR-122 Targeting with LNA/2′-O-Methyl Oligonucleotide Mixmers, Peptide Nucleic Acids (PNA), and PNA-Peptide Conjugates. Rna 2008, 14 (2), 336–346. 10.1261/rna.844108. [PubMed: 18073344]

(35). Hatano A; Makita S; Kirihara M Synthesis and Redox-Active Base-Pairing Properties of DNA Incorporating Mercapto C-Nucleosides. Tetrahedron 2005, 61 (7), 1723–1730. 10.1016/j.tet.2004.12.038.

(36). Faehnle CR; Elkayam E; Haase AD; Hannon GJ; Joshua-Tor L The Making of a Slicer: Activation of Human Argonaute-1. Cell Rep 2013, 3 (6), 1901–1909. 10.1016/j.celrep.2013.05.033. [PubMed: 23746446]

(37). McGann M FRED Pose Prediction and Virtual Screening Accuracy. J. Chem. Inf. Model 2011, 51 (3), 578–596. 10.1021/ci100436p. [PubMed: 21323318]

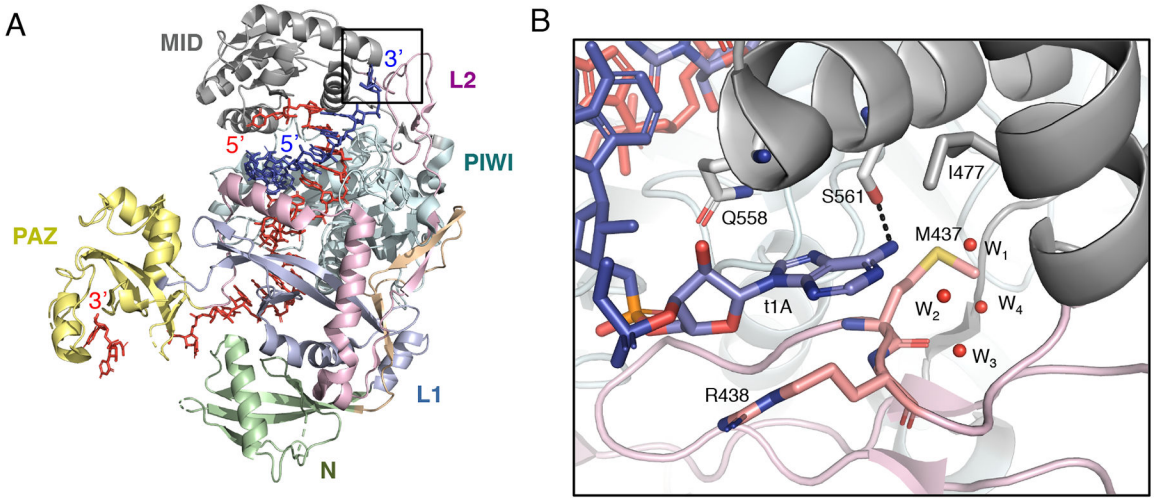

Figure 1.

The t1-adenosine (t1A) binding pocket in human Argonaute2 (hAgo2). (**A**) The crystal structure of hAgo2 with bound guide (red) and target (blue) RNA duplex.[20] The t1A-binding pocket of hAgo2 is encased in a black box. (**B**) Close up of the t1A-binding pocket. Four ordered water molecules within the pocket are labeled as "$W_{\#}$". A hydrogen bonding interaction between the Ser561 residue and the N6 exocyclic amine of t1A is shown with black dashed lines.

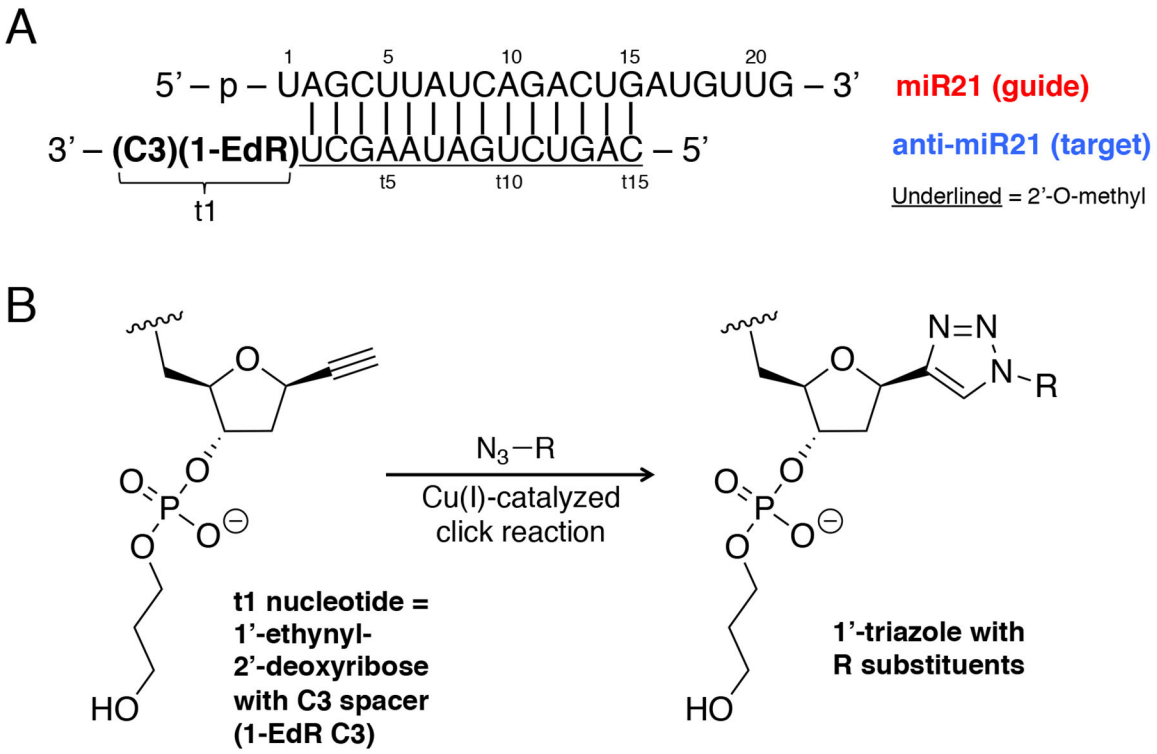

Figure 2.

Design of 15 mer anti-miR21 precursor for CuAAC reactions. (**A**) Sequence of 15 mer, 2'-O-methylated (underlined) anti-miR21 with 1'-ethynyl-2'-deoxyribose monomer at t1 nucleotide. (**B**) Triazole generation at the t1 nucleotide position of anti-miR21 bearing a variety of R substituents.

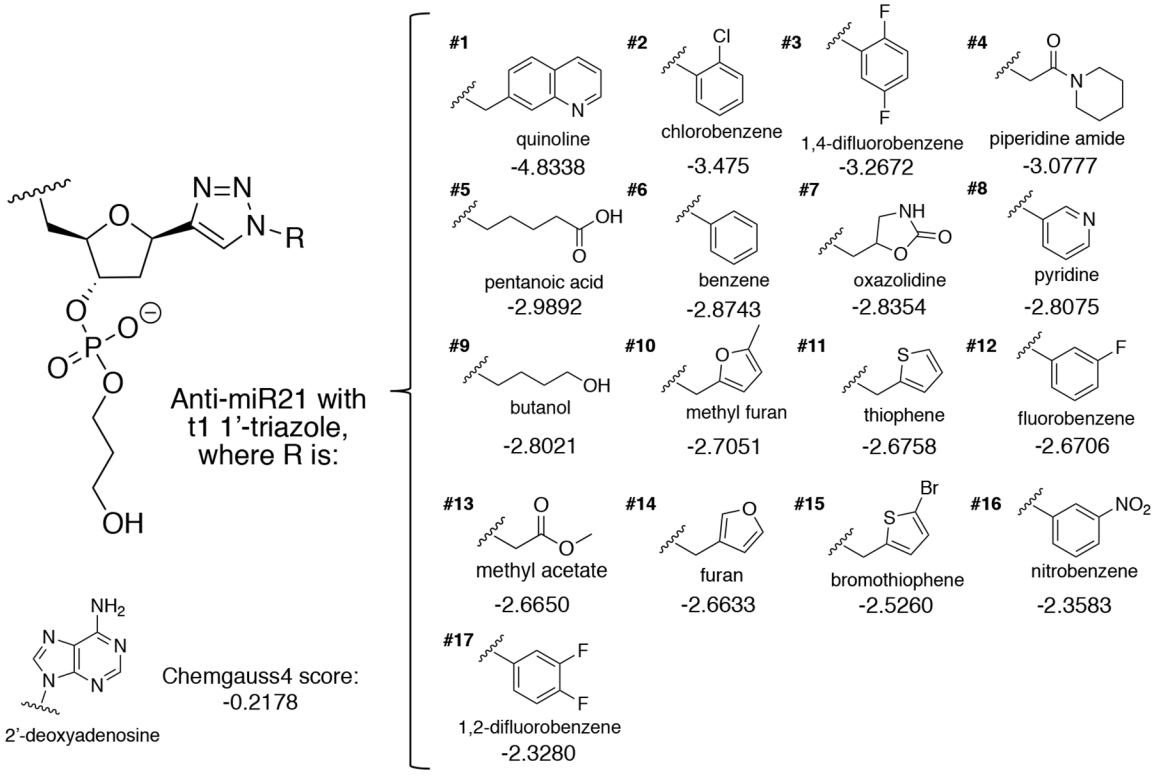

Figure 3.

The 17 triazole candidates identified by computational screening. The 2'-deoxyadenosine ligand and its ChemGauss4 score are shown for comparison.

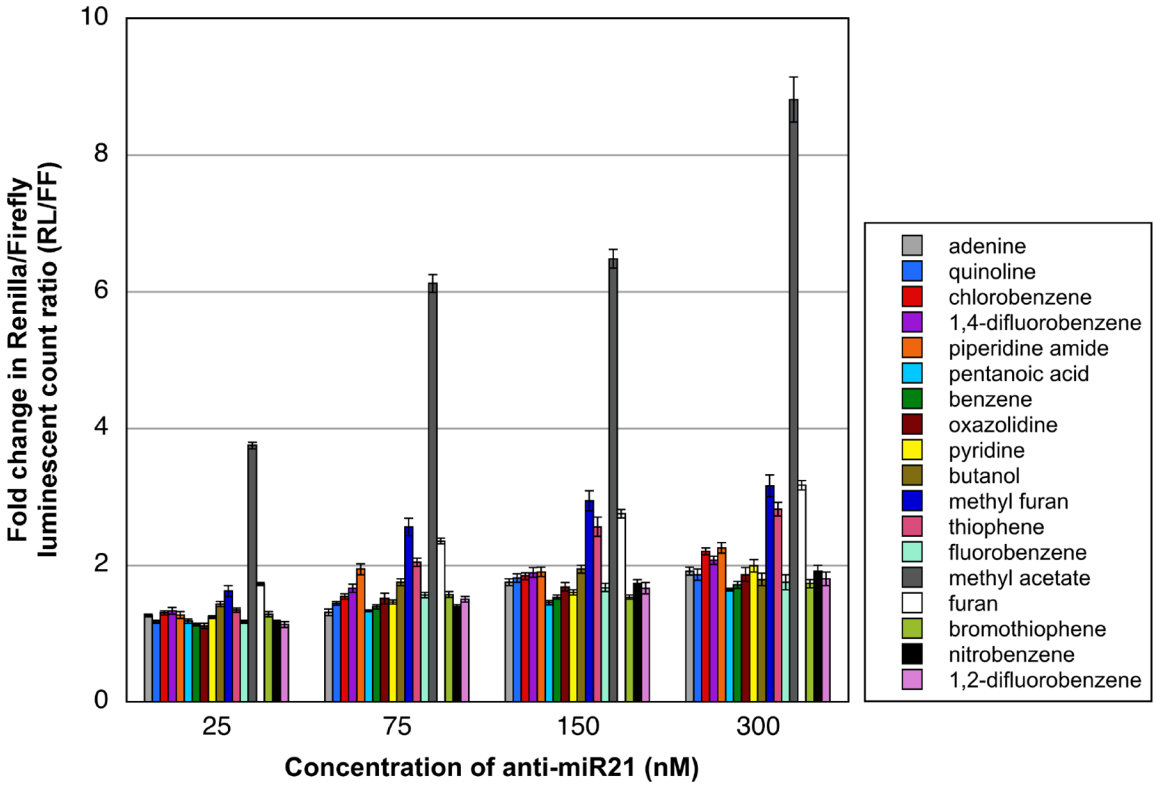

Figure 4.

Potency screening of 17 triazole-modified anti-miR21 in HeLa cells. The bar plots are represented as a fold change in Renilla/Firefly (RL/FF) luciferase activity ratio when normalized to no anti-miR control with a ratio of 1. The error bars are represented as a standard error of the mean (s.e.m.) from at least three biological replicates.

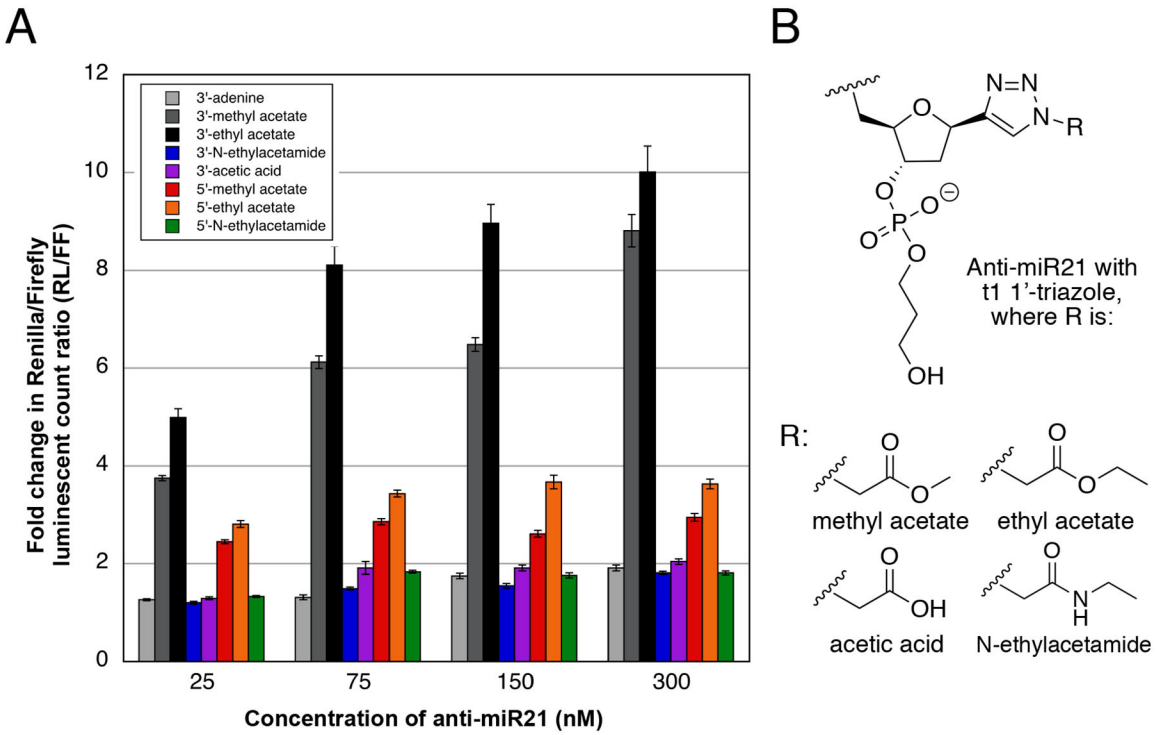

Figure 5.

Structure-activity relationship studies for triazole-modified anti-miR21 in HeLa cells. (**A**) Potency profile of 3'-end triazole modified anti-miR21 with varying substituents along with 5'-end triazole modified anti-miR21. The bar plots are represented as a fold change in (RL/FF) luciferase activity ratio when normalized to no anti-miR control with a ratio of 1. The error bars are represented as a standard error of the mean (s.e.m.) from three biological replicates. (**B**) Structures of triazole modifications at the t1 position of anti-miR21.

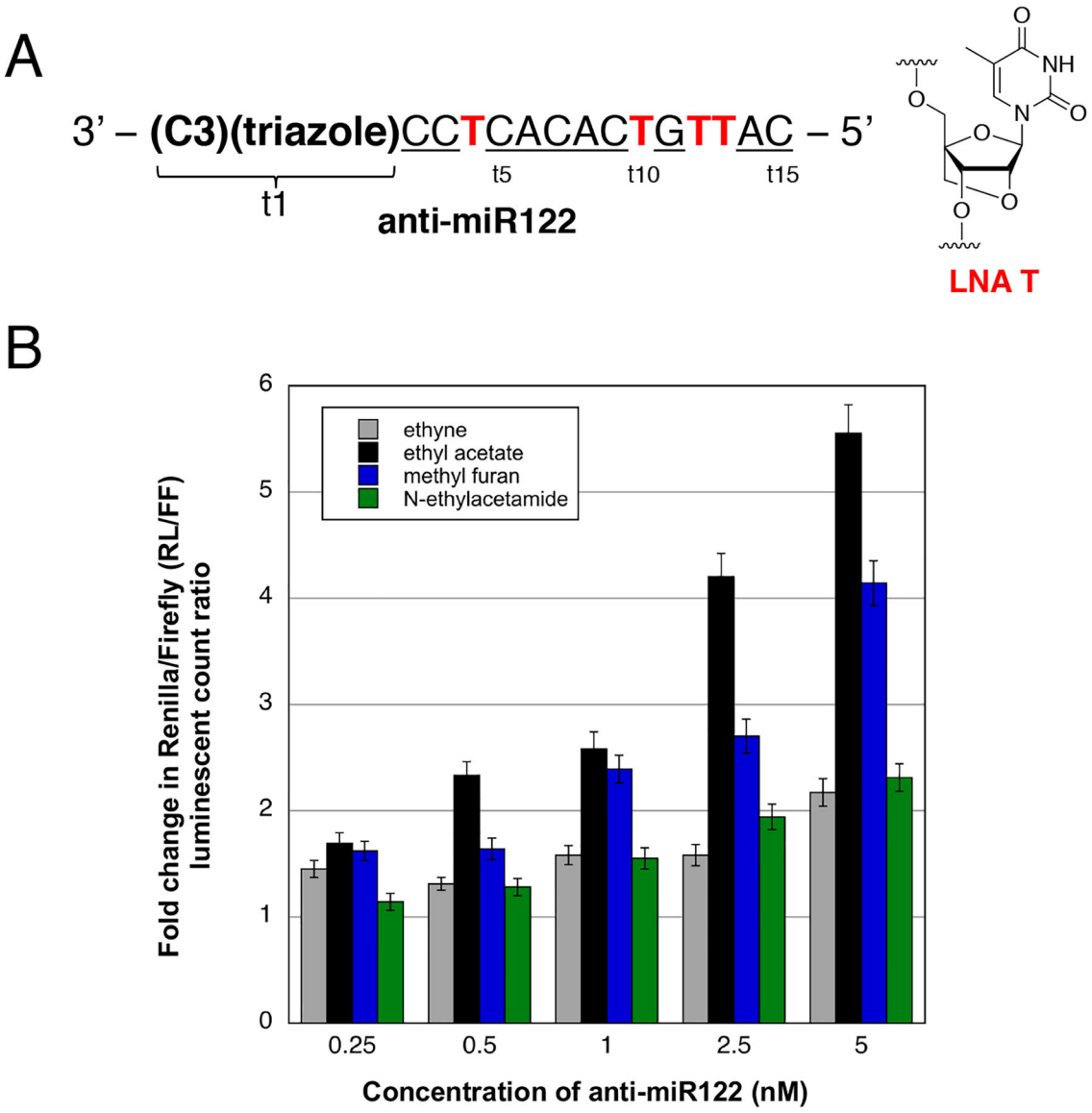

Figure 6.

Potency of t1 triazole-modified anti-miR122 in HuH-7 cells. (**A**) Sequence of anti-miR122 oligonucleotide co-transfected into HuH-7 cells with 100 ng miR-122 reporter plasmid. 2'-O-Methyl (2'-O-Me, underlined) and locked nucleic acid T (LNA T, structure provided) modified nucleotides are underlined and in bold red, respectively. (**B**) Potency profile of t1 triazole-modified anti-miR122 in HuH-7 cells. The bar plots are represented as a fold change in (RL/FF) luciferase activity ratio when normalized to no anti-miR control with a ratio of 1. The error bars are represented as a standard error of the mean (s.e.m.) from three biological replicates.